

Cosmological Galaxy Evolution with Superbubble Feedback I: Realistic Galaxies with Moderate Feedback

B. W. Keller^{1*}, J. Wadsley¹, H. M. P. Couchman¹

¹*Department of Physics and Astronomy, McMaster University, Hamilton, Ontario, L8S 4M1, Canada*

20 August 2018

ABSTRACT

We present the first cosmological galaxy evolved using the modern smoothed particle hydrodynamics (SPH) code GASOLINE2 with superbubble feedback. We show that superbubble-driven galactic outflows powered by Type II supernovae alone can produce L^* galaxies with flat rotation curves with circular velocities ~ 200 km/s, low bulge-to-disc ratios, and stellar mass fractions that match observed values from high redshift to the present. These features are made possible by the high mass loadings generated by the evaporative growth of superbubbles. Outflows are driven extremely effectively at high redshift, expelling gas at early times and preventing overproduction of stars before $z = 2$. Centrally concentrated gas in previous simulations has often lead to unrealistically high bulge to total ratios and strongly peaked rotation curves. We show that supernova-powered superbubbles alone can produce galaxies that agree well with observed properties without the need for additional feedback mechanisms or increased feedback energy. We present additional results arising from properly modelled hot feedback.

Key words: hydrodynamics – methods: N-body simulation – ISM – galaxies: formation – galaxies:evolution – cosmology:theory

1 INTRODUCTION

The theory of galaxy formation is a cornerstone of modern cosmology. Λ CDM accurately predicts the detailed properties of the Cosmic Microwave Background, and the formation of large-scale cosmic structure. Understanding how this yields the small-scale properties of the galaxies we see today and at high redshift requires a good understanding of the physics at play within these individual galaxies: star formation, feedback, gas accretion, etc.

The basic theoretical picture of galaxy formation is now well-established (Rees & Ostriker 1977; White & Rees 1978). The complex details are typically probed through both simulation and semi-analytic techniques (Kauffmann et al. 1999; Bower et al. 2006). Simulators typically employ large-scale cosmological boxes and zoomed in simulations, in which regions sliced out of those larger volumes are re-simulated at higher resolution (Katz & White 1993; Governato et al. 2004; Stinson et al. 2010; Brooks et al. 2011). Recent studies (Dekel & Birnboim 2006; Woods et al. 2014) have shown that the picture of how gas is fed to galaxies is not simple: cold flows can be funneled along filaments in the cosmic

web, bypassing the virial shock and directly supplying gas to the inner galaxy. Gas accretion and expulsion by stellar feedback is fundamental to how galaxies evolve over time, determining not only when and how many stars form, but the kinematic properties of those stars as well.

Stellar feedback has a greater impact than merely regulating star formation by heating the ISM or increasing its turbulence. It has long been understood that the cumulative effects of multiple supernovae can eject gas from the galaxy, powering a galactic outflow or wind (Mathews & Baker 1971; Larson 1974). Galactic winds are common in high-redshift galaxies, and can be seen in the nearby Universe in starburst galaxies (See review by Veilleux et al. 2005). The detection of both blue-shifted rest-frame UV absorption in observations of high redshift galaxies (Weiner et al. 2009; Steidel et al. 2010; Martin et al. 2012) along with broadened $H\alpha$ emission lines (Heckman et al. 1987; Genzel et al. 2011; Newman et al. 2012) strongly suggests the presence of hot, outflowing material surrounding these galaxies. Galactic winds appear to be ubiquitous at high-redshift, and are likely a key factor in the evolution of galaxies in the early Universe. Muratov et al. (2015) estimated that mass loadings for winds peaked at roughly $\eta = \frac{\dot{M}_{\text{wind}}}{M_*} \sim 10$ at high redshift and that a significant fraction of ejected material can escape beyond the virial radius. By ejecting material

* Email: bwkeller ‘at’ mcmaster.ca

from a galaxy’s disc, and storing it in the hot, gravitationally bound circumgalactic medium (CGM), star formation at high redshift can be strongly regulated, while at the same time providing a reservoir of gas that can be accreted at late times, ensuring that star formation at low redshift can continue (Marasco et al. 2012). How this CGM is created is complex, as it is potentially pierced by cold flows of infalling material, outflows from the central galaxy, and the accretion of dwarf satellites.

The first generations of cosmological simulations including baryonic physics (hydrodynamics, star formation, etc.) suffered from a number of serious problems. Nearly every simulation, regardless of halo mass, produced far too many stars, and tended to form these stars too early (Abadi et al. 2003; Governato et al. 2009; Stinson et al. 2010; Brooks et al. 2011). Simulations of disc galaxies produced bulge dominated galaxies rather than the thin discs we observe. Together with the discrepancies seen between large dark-matter only simulations and observations, it appeared that the standard dark energy + cold dark matter cosmology Λ CDM might need to be modified to adequately explain the properties of both individual galaxies and populations of galaxies that we see. Scannapieco et al. (2012) showed these problems were ubiquitous among codes, leading simulators to consider a role for stronger feedback. Early feedback models (e.g. Katz & White 1993) tended to deposit the energy of feedback into a poorly-resolved region of the interstellar medium, subjecting it to over-cooling. Stronger feedback can be achieved by limiting cooling or increasing the total energy. It must also ensure that feedback energy couples strongly to the gas. This strong coupling doesn’t just heat the ISM, or disrupt only the densest regions, but drives outflows that actively remove gas from the disc of the galaxy. The Aquila comparison of 13 different simulation codes and subgrid physics models (Scannapieco et al. 2012) showed that only those cases with strong outflows could produce galaxies with realistic star formation histories. The outflow models used were somewhat ad hoc and extremely aggressive. The cases that were capable of ejecting sufficient gas from the galaxy disc to moderate the stellar mass of the halo still failed to produce stellar discs and largely shut down low redshift star formation.

Galactic winds have been a part of cosmological galaxy simulations for some time (Springel & Hernquist 2003), and recent simulations have investigated these winds in detail. Anglés-Alcázar et al. (2014) showed that these winds can dramatically alter the star formation history, kinematics, and morphology of galaxies at redshift 2. By explicitly creating galactic winds with a variety of mass-loadings and wind velocities, they showed that strong winds are essential to producing the gas-rich, extended, and turbulent discs that are typically observed in high redshift star forming galaxies. Unfortunately, without simulations to $z = 0$, interpreting exactly how these high-redshift winds impact present-day galaxies is difficult. If outflowing material falls back onto the galactic disc within a Hubble time, the effects of high-redshift winds may be seen in the form of increased star formation and inflows at low redshift.

A key question remains: What processes set the mass loading and velocity of these winds? Early work tied galactic outflows to the SNe energy (Springel & Hernquist 2003). Some studies (e.g.

Murray et al. 2005; Krumholz & Thompson 2013) have suggested that radiation pressure is needed to drive sufficient galaxy-scale winds. Others argue that galactic winds could be powered by cosmic ray buoyancy (Ipavich 1975; Breitschwerdt et al. 1991; Socrates et al. 2008).

Today, multiple different models of strong feedback have begun to produce galaxies with the correct number of stars (Aumer et al. 2013), reasonable star formation histories (Stinson et al. 2013; Agertz & Kravtsov 2014; Munshi et al. 2013), and correct morphologies (Guedes et al. 2011; Brook et al. 2012; Christensen et al. 2014). Unfortunately, many of these successes have come at the cost of increasing complexity in star formation and feedback methods, crude assumptions regarding the physics of the feedback-heated gas and somewhat arbitrary increases in the feedback energy per unit mass in stars.

In many cases, strong feedback simply means more energy. Many modern feedback models augment the energy input from Type II supernovae ($\sim 10^{51}$ erg per star above $8 M_{\odot}$), with that arising from stellar winds, UV ionization, supermassive black holes (SMBH), or radiation pressure (Vogelsberger et al. 2013; Agertz & Kravtsov 2014). Feedback models such as Stinson et al. (2013) group these sources of energy as early stellar feedback. Since the first supernovae occur ~ 4 Myr after star formation, these feedback mechanisms begin depositing feedback before SN-only methods would. Unfortunately, how much energy from these early feedback effects actually couples to the surrounding ISM rather than radiating away is highly uncertain. In fact, even the coupling of comparatively simpler SN feedback still is a matter of some debate. Many new feedback models (Ageretz et al. 2013; Aumer et al. 2013; Hopkins 2013) treat each of these feedback mechanisms explicitly, modelling the input of energy and momentum from each component separately.

In addition to increasing the total amount of energy deposited by stellar feedback, these models often also include components designed to prevent energy from feedback radiating away (a problem discussed thoroughly in Thacker & Couchman 2000). The energy can be prevented from cooling completely for a while (Stinson et al. 2013) or it can be initially placed into a non-cooling reservoir that leaks back into regular thermal energy (Ageretz et al. 2013). Alternately, depositing thermal feedback into a sufficiently small mass, allows it to always heat gas to the same high temperature where cooling times are long (Dalla Vecchia & Schaye 2012). Depositing feedback as kinetic avoids initial radiative losses (Springel & Hernquist 2003; Agertz et al. 2013; Hopkins 2013).

While these techniques do help solve the overcooling problem, they all come with some drawbacks. Fixed-temperature thermal feedback is stochastic, and requires the additional free parameter of the feedback temperature. Cooling shutoffs completely disable radiative losses, where in nature these losses are suppressed in some regions but can remain strong in others, depending on the structure of the ISM and the clustering of stars. Kinetic feedback is almost always paired with a temporary decoupling of hydrodynamic forces on feedback-accelerated gas. This is necessary to prevent this gas from shock-heating and potentially reintroducing the overcooling problem (as shown by Creasey et al. 2011; Durier & Dalla Vecchia 2012). Decoupling allows winds to

escape. However, this makes it impossible to study the detailed behavior of these winds, and how they interact with the ISM. This makes the mass loading an imposed parameter.

Of these methods, [Dalla Vecchia & Schaye \(2012\)](#) showed the interesting result that, for supernovae alone, depositing feedback energy into a pre-specified amount of mass, without any cooling shutoffs, can give reasonable star formation rates and strong galactic outflows in isolated galaxies. [Keller et al. \(2014\)](#) argued that what sets this mass is thermal conduction in superbubbles, and used that mechanism to build a new way of simulating supernovae feedback that lacked the resolution dependence, additional complexity, and ad-hoc additions of many current feedback models. By focusing on superbubbles, and the evaporation of cold gas to determine mass loading, superbubble feedback gives realistic gas behavior, and is effective at both regulating star formation and driving galactic outflows without introducing free parameters.

The original McMaster Unbiased Galaxy Simulations (MUGS; [Stinson et al. 2010](#)) showed that with stellar feedback, the observed color-magnitude relationship and Tully-Fisher relation could be produced in simulated L^* galaxies. It failed, however, to produce galaxies with the correct stellar mass fraction and star formation history, overproducing stars over the entire cosmic history, and grossly overproducing them at high redshift. It also produced galaxies with bulge-to-disc fractions larger than those seen in nature, and with sharply peaked rotation curves. [Stinson et al. \(2013\)](#) showed that the addition of early stellar feedback could alleviate most of these problems. That model does not take into account the potentially complex coupling of stellar winds or radiation pressure to the surrounding ISM. Instead, a substantial (fixed) fraction of the stellar bolometric luminosity was applied as feedback heating.

In this paper, we begin first with an overview of the simulation methods used, both gas microphysics and the star formation and feedback techniques. We then present the results of a suite of 4 simulations using an initial condition from the MUGS sample, each generated with different stellar feedback models or energetics. The resulting galaxy properties, as well as the halo evolution are examined over the lifetime of the galaxy. Finally, we discuss how the superbubble-driven outflows change with time, and how they ultimately result in a realistic galaxy at the present epoch.

2 METHODS

These simulations were run using a modern update to the SPH code GASOLINE ([Wadsley et al. 2004](#)), GASOLINE2. The changes in this new code include a sub-grid model for turbulent mixing of metals and energy ([Shen et al. 2010](#)), and a modified pressure force form similar to that proposed by [Ritchie & Thomas \(2001\)](#) which is functionally equivalent to [Hopkins \(2013\)](#). These changes solve the problems seen in Kelvin-Helmholtz and blob destruction tests with SPH ([Agertz et al. 2007](#)). These and other features are discussed in [Keller et al. \(2014\)](#). Accurately modelling mixing in multiphase gas is essential for accurately simulating the ISM and CGM.

2.1 Simulations

For this initial study, we have selected the initial conditions from one of the original MUGS galaxies. We selected an intermediate-mass halo, g1536, allowing us to compare to a number of other studies that have examined this particular halo (e.g. [Stinson et al. 2013](#); [Woods et al. 2014](#)). At $z = 0$ this halo has a virial mass of $8 \times 10^{11} M_\odot$ and a spin parameter of 0.017. It had its last major merger at $z = 2.9$. We have a gas mass resolution of $M_{gas} = 2.2 \times 10^5 M_\odot$, and use a gravitational softening length of $\epsilon = 312.5$ pc. The details of how this IC was created can be found in [Stinson et al. \(2010\)](#). We choose to focus on a single galaxy for this paper as it allows us to make a direct comparison of the impact feedback physics makes with relatively little expense. Naturally, this limits our ability to comment on population-wide effects. We leave this discussion for a forthcoming paper in which we introduce 17 additional L^* galaxies.

We compare four test cases using the same initial conditions: no stellar feedback (an absolute lower bound for looking at the effects of feedback); superbubble feedback (our fiducial case); blastwave feedback (the feedback method used in [Stinson et al. \(2010\)](#), first described in [Stinson et al. 2006](#)); and superbubble feedback with double the standard feedback energy (2×10^{51} erg per SN). The high feedback energy case uses more feedback than is predicted by [Leitherer et al. \(1999\)](#), but is within the range of feedback energies currently being used in cosmological simulations ([Schaye et al. 2015](#); [Agertz & Kravtsov 2014](#); [Vogelsberger et al. 2013](#)).

Halos were found in each of the simulations using the Amiga Halo Finder (AHF; [Knollmann & Knebe 2009](#)).

2.2 Star Formation and Feedback

Our suite of simulations use a range of different feedback processes. For all of the simulations shown in this paper, we use a common star formation prescription. Stars are formed at a rate proportional to the local free-fall time of gas, such that

$$\dot{\rho}_* = c_* \frac{\rho_{gas}}{t_{ff}} \quad (1)$$

For each of these simulations, we used an efficiency parameter $c_* = 0.1$, the value used by [Stinson et al. \(2013\)](#). Stars are allowed to form in a converging flow when gas is cooler than 1.5×10^4 K, and with a density set to that allowed by the gravity resolution, $\rho = M_{gas}/\epsilon^3 = 9.3 \text{ cm}^{-3}$.

The amount of supernova feedback per unit stellar mass is determined using a [Chabrier \(2003\)](#) IMF. With $\sim 10^{51}$ erg per supernova this gives $\sim 10^{49}$ erg M_\odot^{-1} . A notable difference between this simulation and those of [Stinson et al. \(2013\)](#) and others is that we do not include early feedback, processes such as stellar winds and radiation that can inject energy before supernovae occur ~ 4 Myr after the first massive stars form. A primary role for early stellar feedback is to disrupt the densest molecular gas. In these simulations, this dense molecular gas cannot be resolved, never being formed (and thus it does not form or need to be destroyed).

The feedback recipe used in our main simulations is the superbubble method presented in [Keller et al. \(2014\)](#). This method deposits feedback into resolution elements in a brief multi-phase state. These particles each have separate

specific energies, masses and densities, for the hot bubble and surrounding cold ISM, which includes the swept up shell. This allows the method to calculate a separate density and cooling time with the respective densities for each phase, rather than the average density of both phases. Multiphase particles are also prevented from forming stars: the average temperature of the two phases is essentially always above our temperature threshold for star formation. More details on this method can be found in Keller et al. (2014).

The addition of thermal conduction and evaporation introduces some additional time step constraints in order to ensure the stability of integration. However, since the thermal conduction rate is capped by the saturation imposed by the electron soundspeed, this time step is at worst 1/17 the Courant time step. In fact, we see an overall speedup when using superbubble vs. blastwave feedback, as gas can no longer exist in the regime of high density and temperature (and thus small Courant times). The average computation time per step was $\sim 25\%$ faster using superbubble feedback compared to blastwave feedback. These benefits are dominant late in the run, as the total amount of dense gas becomes larger. We do see some slight increased cost early in the run, with a slowdown of $\sim 50\%$ before $z=4$. The additional time-step constraints here are similar to the time-step constraints required for other methods as well, such as decoupled kinetic winds (Springel & Hernquist 2003).

2.3 Gas Cooling and Physics

We adopt the same gas cooling physics as a number of past simulations using GASOLINE (Stinson et al. 2013; Keller et al. 2014). The method for cooling we use here was originally presented in Shen et al. (2010). Our simulations use cooling rates from CLOUDY (Ferland et al. 2013), and include a redshift-dependent UV background, Compton cooling, and primordial and metal cooling from 10 to 10^9 K. This sets these simulations apart from many past simulations (Governato et al. 2009; Brook et al. 2011; Guedes et al. 2011), which did not include high temperature metal cooling. We impose an artificial pressure floor, using a method described by Robertson & Kravtsov (2008) to prevent spurious Jeans fragmentation (as cold, dense gas has both Jeans length and Jeans mass below the resolution limit of our simulation). We also enforce that the minimum SPH smoothing length a particle may have is $\epsilon/4$. This is equivalent to a density floor of 400 cm^{-3} (note that for two-phase superbubble particles, this is the maximum *mean* density). These are comparable to the parameter choices in another recent re-simulation of the MUGS initial conditions, Stinson et al. (2013).

3 RESULTS

3.1 Redshift zero Disc Properties

As can be seen in Figure 1, the galaxy produced with superbubble feedback is disc-dominated and blue. The stellar disc in the case without feedback is nearly non-existent, with an ellipsoidal morphology. The superbubble disc appears somewhat thicker and truncated compared to the disc produced with blastwave feedback. The truncation can be

seen in the reduced stellar scale length of the superbubble galaxy, 2.9 kpc vs. 3.8 kpc for the superbubble vs. blast-wave galaxies. The thickening appears to be quantitatively insignificant, however, as both discs have stellar scale heights of 0.9 kpc. This may be due to the disc being disrupted at large radii, where the surface densities are lower, allowing superbubbles to grow larger and escape more easily. The increased feedback case is interestingly somewhat tilted compared to the rotation of the halo as a whole.

The gas component of this galaxy can be seen in Figure 2. The superbubble feedback is clearly much more effective at ejecting gas from the disc, creating a halo of clumpy HI gas. In the doubled feedback case, the disc is heavily disrupted, with no spiral structure visible in either the stellar or gas density images. Thus the larger stellar disc is directly related to a more extended gaseous disk.

The rotation curve in Figure 3 shows that this ejection also gives a flattened rotation curve without the central peak seen in simulations with blastwave or no feedback. This tells us that the mass distribution is much less centrally concentrated when superbubble feedback is used, more evidence that superbubble feedback is effective in preventing bulge formation.

One of the primary problems in older simulations was a much larger bulge-to-total fraction based on a kinematic decomposition. We adopt the same kinematic decomposition as the original MUGS study. We calculate, for each star within the halo, a circularity parameter, which is simply the ratio of the specific angular momentum component perpendicular to the disc (j_z) and the specific angular momentum for a perfect circular orbit in the same potential that the star sees j_{circ} . As in the original MUGS study, we identify bulge stars as having $j_z/j_{\text{circ}} < 0.7$ and orbital radii of < 5 kpc. We find, using these criteria, that our fiducial B/T ratio at $z = 0$ is 0.09, slightly smaller than the Milky Way's ~ 0.14 , and greatly reduced compared to the 0.55 found in the original MUGS paper, and well within the observational constraints from Allen et al. (2006). As these numbers, and the distribution of this circularity parameter found in Figure 4 show, the vigorous expulsion of central gas with superbubble feedback is a powerful bulge prevention and destruction mechanism. Each of the 13 samples from the Aquila project (Scannapieco et al. 2012) suffered from either from a bulge-dominated stellar circularity profile, or from a massively peaked (or in some cases simply too high) rotation curve. Even the three cases that managed to produce a reasonable stellar mass fraction (each of these generated strong outflows, either through SMBH feedback or wind decoupling) still failed to produce disc-dominated galaxies. Of their sample, only four cases had more than 40% of the stellar mass in disc stars, but all of these cases massively overproduced stars.

The ejection of gas is evident if we look at the baryon content of the interior part of the halo, where the disc resides, in this case, simply material within $0.1R_{\text{vir}}$. With superbubble feedback, the baryon fraction of this inner region is 0.30, reduced from 0.37 without feedback, and 0.35 with blastwave feedback. This means that nearly 20% of the baryons that would be available to form stars have been blown out of the galaxy disc, roughly twice the amount that was removed by the older feedback model. The baryon deficit in the superbubble is comparable to the total stellar mass

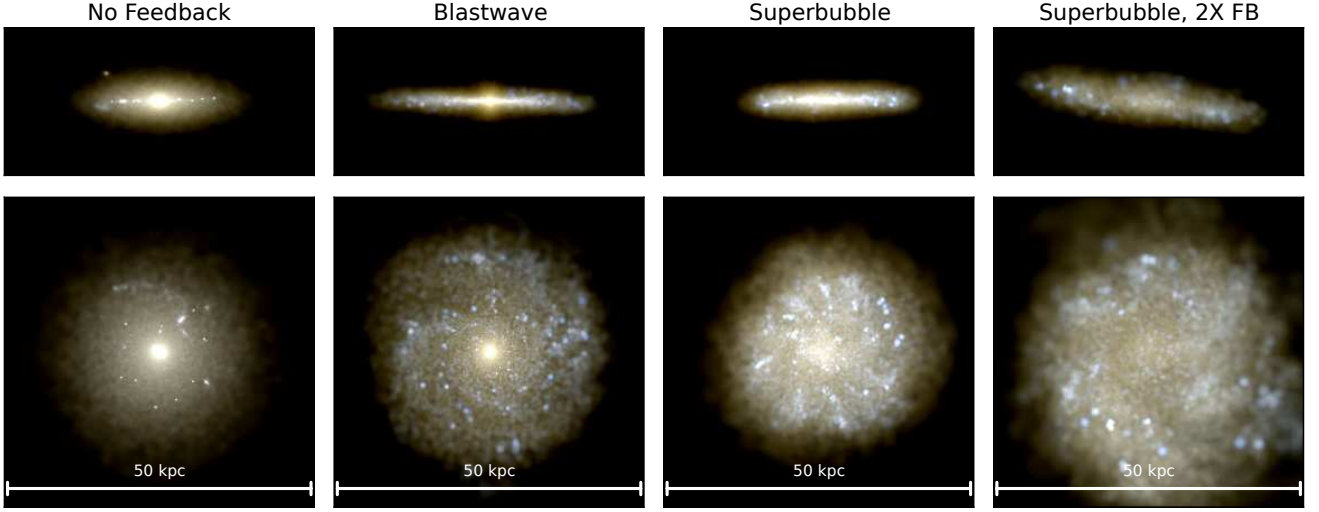


Figure 1. Mock stellar image of each galaxy at $z = 0$. The top row shows the galaxies edge-on, while the bottom shows them face-on. The no-feedback case shows very little disc, while the blastwave feedback case has a thin disc with a prominent bulge. The superbubble galaxy appears nearly bulgeless, composed only of a truncated disc. Note also that the superbubble galaxy is bluer than the blastwave or no-feedback galaxies, evidence of a younger stellar population.

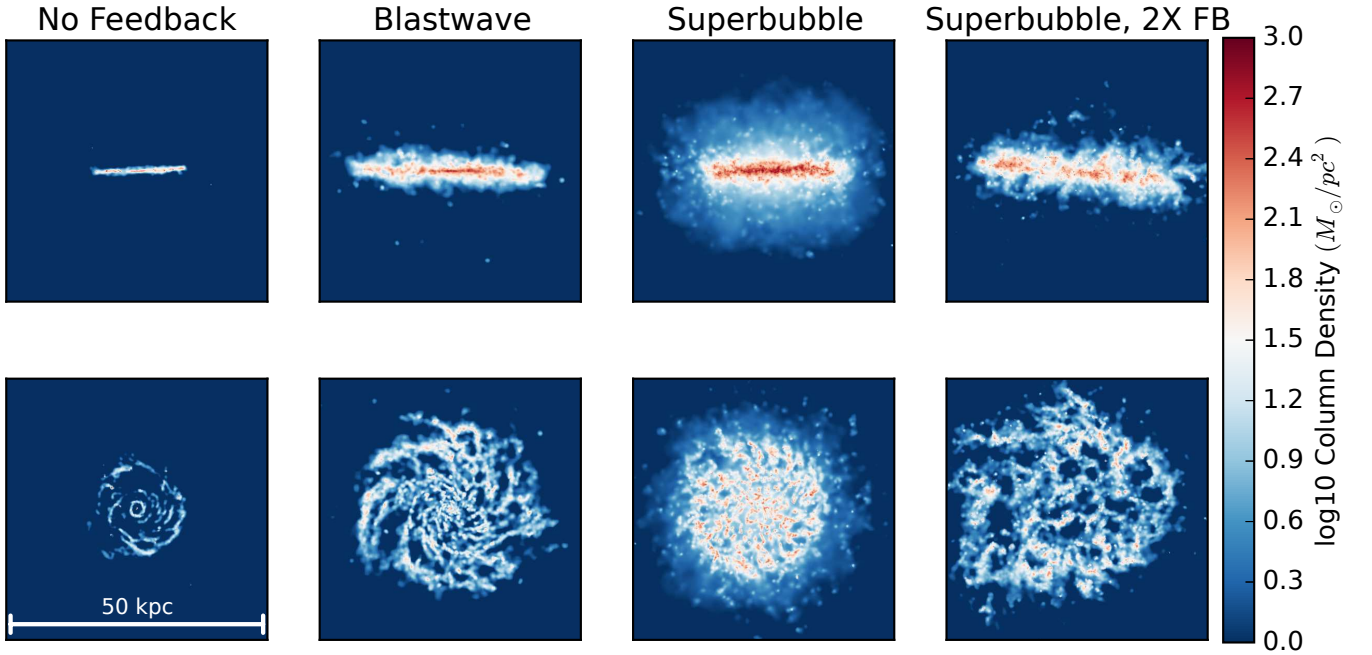


Figure 2. HI column density for the four test cases at $z=0$. The no feedback case has exhausted nearly all of the gas within the disc, leaving only diffuse wisps. The two superbubble cases (especially with doubled supernova energy) have lofted a large amount of gas out of the disc, and some entrained dense clumps can be seen in this outflowing material. The superbubble gas discs are much more flocculent than the blastwave disc, and where the feedback energy is doubled, the disc is strongly disrupted.

| Simulation | M_{vir} | M_{gas} | M_{star} | $M_{bary,0.1vir}$ | M_{bulge} | M_{disc} |
|--|-----------------------|-----------------------|-----------------------|-----------------------|--------------------|-----------------------|
| No Feedback | 7.94×10^{11} | 6.21×10^{10} | 7.42×10^{10} | 8.09×10^{10} | 9.34×10^9 | 2.88×10^{10} |
| Blastwave Feedback | 7.99×10^{11} | 8.05×10^{10} | 5.11×10^{10} | 7.94×10^{10} | 8.09×10^9 | 1.75×10^{10} |
| Superbubble Feedback | 8.02×10^{11} | 1.19×10^{11} | 1.84×10^{10} | 6.25×10^{10} | 1.14×10^9 | 1.15×10^{10} |
| Superbubble, $2 \times 10^{51} \text{ erg/SN}$ | 7.96×10^{11} | 1.20×10^{11} | 1.09×10^{10} | 4.92×10^{10} | 5.96×10^8 | 6.98×10^9 |

Table 1. Halo components at $z = 0$. M_{disc} and M_{bulge} are the determined by the angular momentum of the stars (as detailed below). All masses are in M_{\odot} .

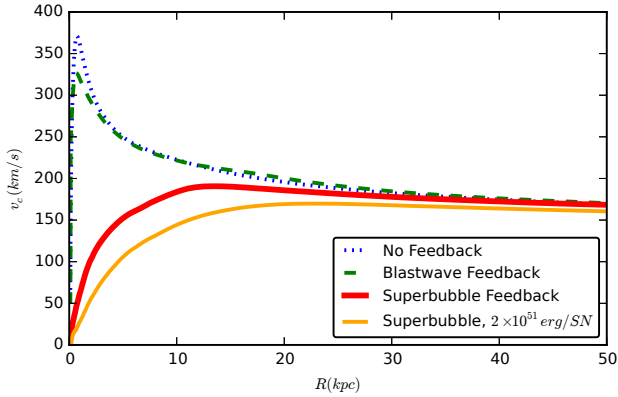


Figure 3. Rotation curves for each of our test cases. As is clear, the superbubble cases have much lower central concentrations, giving a rotation curve that rises to a flat 200 km/s. The peaked rotation curves in the cases with blastwave or no feedback are a result of their failure to remove low angular momentum gas at high redshift, giving bulge-dominated, centrally concentrated galaxies.

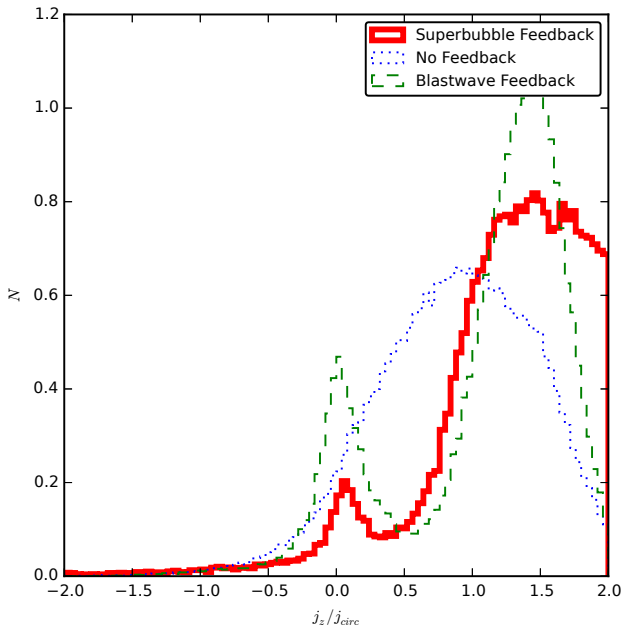


Figure 4. Histogram of stellar orbit circularity. The bimodal distribution shows the bulge component, with a circularity near 0, and the disc component, with a circularity near 1. Note that without feedback, this bimodality disappears, as the galaxy morphology becomes spheroidal. The values here are normalized so that each curve has a total integral of unity. As is clear, very few stars produced in a galaxy with superbubble feedback have low angular momentum, giving us a disc-dominated galaxy.

of the galaxy (the fiducial case has a $1.5 \times 10^{10} M_\odot$ deficit in baryons (compared to the no-feedback case), and a total stellar mass of $1.8 \times 10^{10} M_\odot$).

Of what remain, only 29% of the baryonic mass in the superbubble galaxy disc is in stars, compared to 63% in the blastwave galaxy, and 89% in the no feedback galaxy. The basic properties of each halo can be found in table 1.

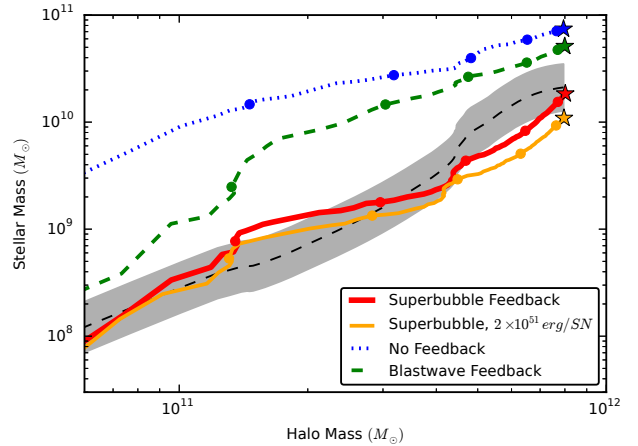


Figure 5. Stellar mass growth as a function of the total halo mass. The grey band and black dashed curve show mean values and uncertainties from the abundance matching results of Behroozi et al. (2013). The points show values at redshifts 3, 2, 1, 0.5, and 0.1. The stars show the final values at redshift 0. For essentially the entire evolution of the halo, both the no feedback galaxy and the blastwave galaxy overproduce stars.

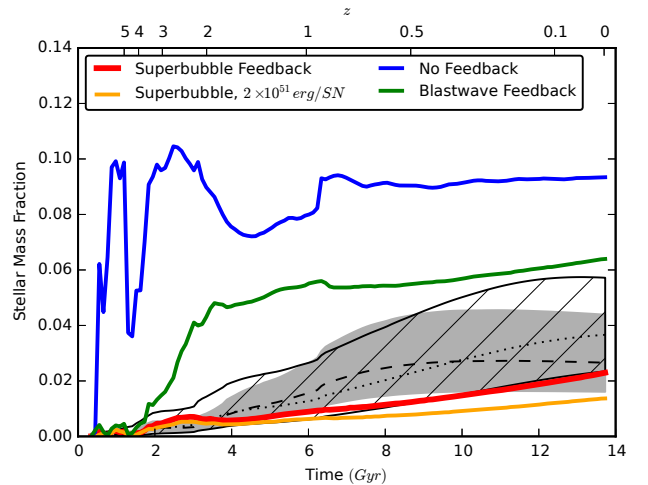


Figure 6. Stellar mass fraction as a function of time/redshift. As in figure 5, only the fiducial superbubble run produces stellar mass fractions within observed uncertainties for the entire history of the halo. The grey band is as in figure 5, and here we also show, in the hatched region with the dotted curve, values and uncertainties from Moster et al. (2013). The dip that can be observed in the no feedback case at high redshift come from the growth of the halo, as it accretes dark matter dominated dwarves.

3.2 Halo Evolution and Star Formation

Ejecting baryons from the disc is essential to producing galaxies that fit the M_*/M_{halo} relationship predicted by Behroozi et al. (2013), Moster et al. (2013) and others. As Figures 5 and 6 show, the galaxies either lacking feedback or using blastwave feedback alone fail to regulate star formation, diverging from the expected abundance matching relation at $z \sim 3$ for the blastwave, and before $z = 5$ without feedback, giving galaxies that lie above the abundance-

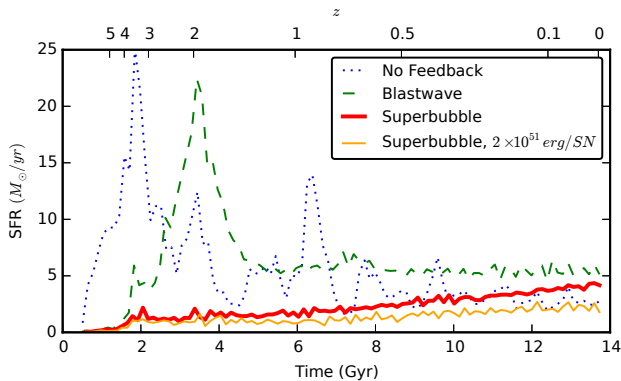


Figure 7. Star formation rates for all 4 simulations. The low star formation rate seen after $z = 1$ in the no feedback case is due simply to the high z star formation consuming most of the available gas.

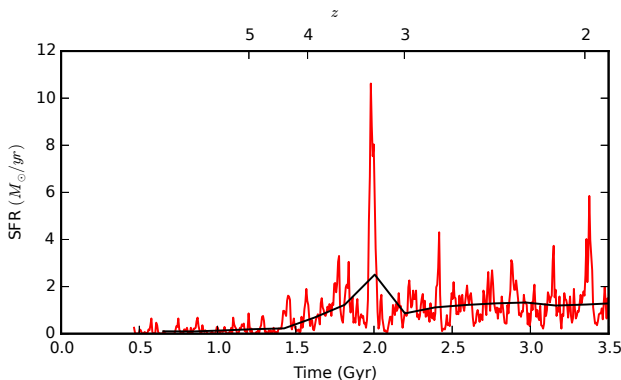


Figure 8. Star formation rate up to $z = 2$ for our superbubble galaxy. As is clear, when sampled on short (7 Myr) timescales, the star formation rate in the superbubble galaxy is characterized by strong bursts, despite its quiescent behavior averaged over longer timescales.

matching relationships over nearly their entire history and mass evolution. With superbubble feedback, this galaxy lies within the range of observed stellar masses over its entire evolution, although on the low side of this range at low redshift. Arbitrarily increasing feedback energies, despite having reasonable star formation rates near $z = 0$, under produces stars for most cosmic history, giving stellar masses *lower* than predicted by abundance matching. Stellar and total masses were calculated for the region inside R_{vir} . As the halo grows over time, brief reductions in the stellar mass fraction can be seen for the no-feedback and blastwave feedback halos in Figure 6, simply by the accretion of gas and dark matter that has not yet made it to the galaxy disc. Once these mergers complete, the stellar fraction rate leaps up once again because of the new supply of gas. The relative flatness in this figure at low redshift is reflected in the relative flatness in the star formation rate, shown in figure 7. This is simply a side effect of the massive star formation rates at high redshift: the bulk of star forming gas has been consumed, and thus star formation has slowed.

The star formation rate, in bins of 150 Myr, is shown

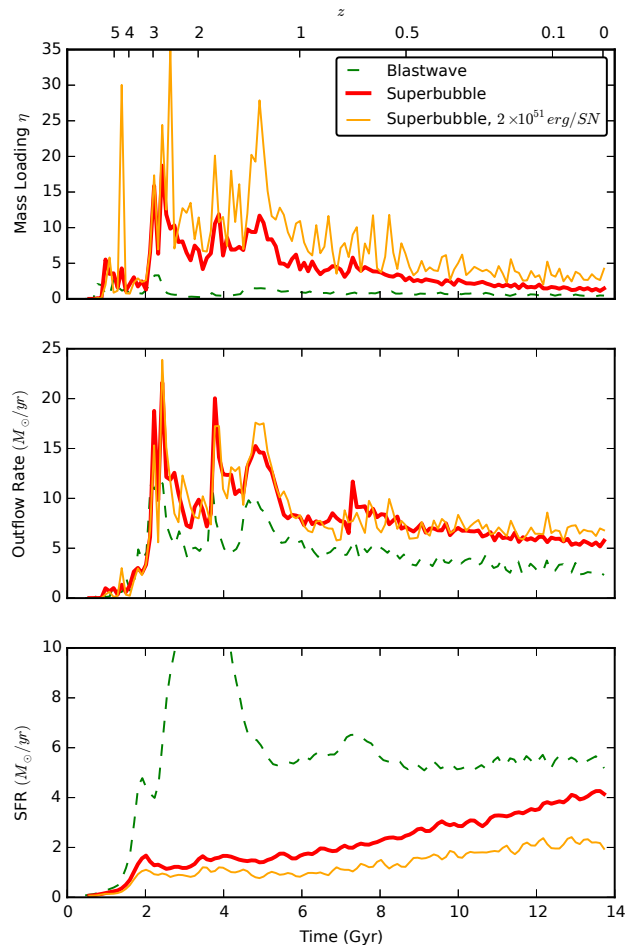


Figure 9. Galactic wind mass-loading and outflow rates for each feedback model. As is clear, superbubble feedback powers winds with significantly higher mass-loadings, and, despite forming less than half as many stars the blastwave galaxy, results in more total outflowing gas. This is key to the regulatory power of superbubbles. Despite the peak in outflow rate in the blastwave case between $z = 4 - 1.5$, the massively increased star formation rate seen in the the smoothed SFR during this time (bottom plot) means that the mass-loadings never go above 5, and baryon expulsion is inefficient.

in Figure 7. With no feedback, or blastwave feedback, star formation is extremely vigorous before $z = 2$, slowing at low redshift as gas available for star formation is exhausted. With superbubble feedback, star formation is relatively constant over nearly the entire history of the halo, with only a gradual increase towards $z = 0$. This apparent quiescence is a function of the large time window over which we are averaging our star formation rate. In Figure 8, you can see clearly that despite having an average star formation rate of $\sim 1 \text{ M}_\odot \text{ yr}^{-1}$, this is punctuated by bursts of star formation of as much as $\sim 10 \text{ M}_\odot \text{ yr}^{-1}$. Very similar results were seen in Muratov et al. (2015), where bursts of star formation are followed by peaks in the outflow rates. This burstiness is an important if stellar feedback is to drive galactic winds: to generate large superbubbles, star formation must be clustered in both space and time. Whether these bursts of star formation are able to effectively remove baryons from the

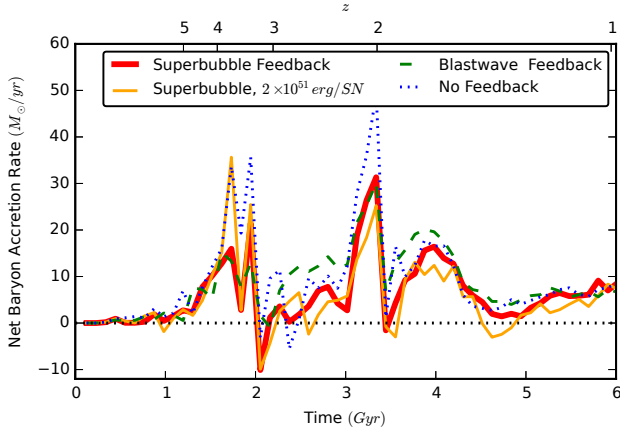


Figure 10. Net baryonic accretion (stars and gas) for each test case. It is clear that superbubble feedback expels baryons much more effectively than the blastwave feedback model (although even weak feedback does help somewhat compared to no feedback whatsoever).

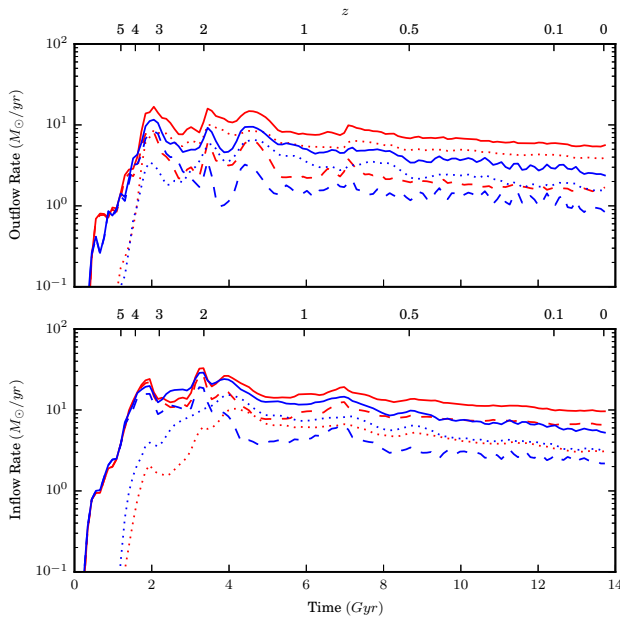


Figure 11. Inflow and outflow rates for superbubble (red) and blastwave (blue) run. The solid lines show the total inflow rate, while the dashed and dotted lines show rates for cold and hot gas (above/below 10^5 K) respectively.

disc ultimately depends on the mass loading of the winds that they drive.

3.3 Outflow Analysis

Star formation in the disc drives hot, fast-moving outflows from the central star forming regions. These outflows have temperatures of $\sim 2 \times 10^7$ K as they leave the disc, and also entrain some cold material with them. Typically outflow velocities are a few hundred km/s, less than the escape velocity

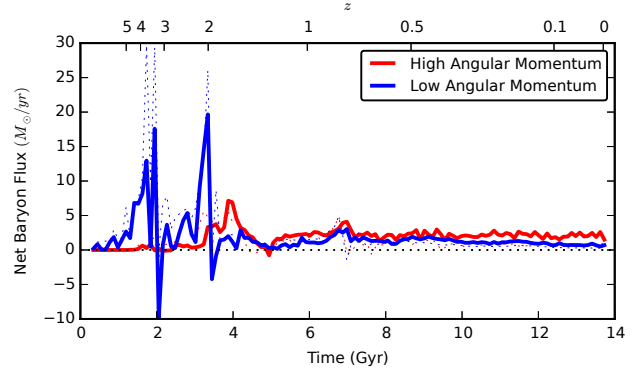


Figure 12. In all four test cases, including the fiducial superbubble run shown above by the solid curve, and the no-feedback case shown by the dotted curve, the vast majority of low angular momentum material, with specific angular momentum $j_z < 500$ kpc km/s, is accreted by $z = 2$. The accretion of high angular momentum material, with $j_z > 1500$ kpc km/s rises to peak at $z = 2$, and continues to accrete $\sim 2 M_\odot/\text{yr}$ at $z = 0$. As can be seen here, the net flux of low angular momentum material at high redshift is suppressed, while the accretion of high angular momentum material at low redshift is actually *enhanced* by superbubble feedback.

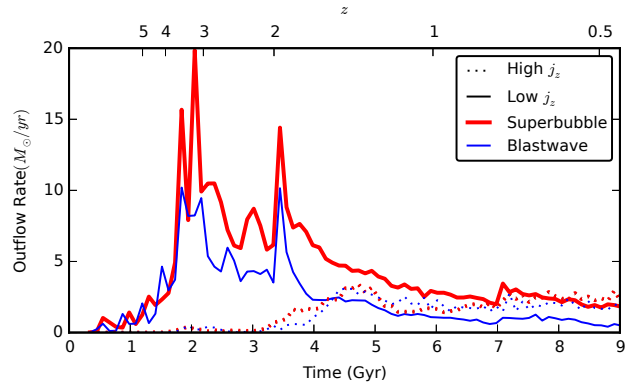


Figure 13. High-redshift winds preferentially remove low angular momentum material. As can be seen here, significantly more low angular momentum material is removed by superbubble feedback than by the weaker blastwave feedback, but the amount of ejected high-angular momentum material is roughly equal.

of the halo, but sufficient to propel gas to large radii before it begins to fall in again.

We calculated inflow and outflow rates and velocities by examining particles within a spherical shell, with inner radius $0.1R_{\text{vir}}$ and outer radius R_{vir} (giving a shell of thickness $0.9R_{\text{vir}}$). We use the $\bar{\rho} = 200\rho_{\text{crit}}$ definition for R_{vir} . Particles with $v_r < 0$ are inflowing, while those with $v_r > 0$ are outflowing. Within this shell, the mass flux is determined simply as:

$$\dot{M} = \sum_{r_i \in \text{shell}} \frac{M_i v_i}{0.9R_{\text{vir}}} \quad (2)$$

As figure 9 shows, the outflow behavior of this galaxy is fundamentally different when superbubble feedback is used. The wind mass loading factor $\eta = \dot{M}_{\text{outflow}}/\dot{M}_*$, a measure

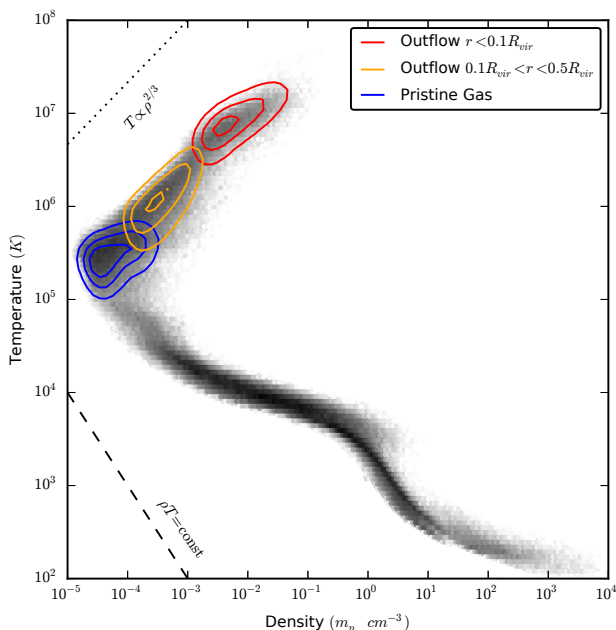


Figure 14. Phase diagram of gas in the halo at $z = 0$. The hot, coronal gas with temperatures above 10^5 K contains roughly 40% of the gas mass in the halo. This gas is a mixture of virial-shocked pristine gas, which has never been within the interior $0.1R_{vir}$, and outflowing material ejected from the galaxy. This buoyant, high-entropy gas exits the galaxy at high temperature, and cools adiabatically as it rises through the CGM. The three colored contours show the major components of this hot coronal gas. Pristine gas, never falling within the interior, is shown in blue. Young superbubbles, not yet having broken out of the galaxy, are shown in red. Outflowing material that was once inside the galaxy but is now cooling adiabatically as it rises through the CGM can be seen in orange. The contours show the 1.5%, 1%, and 0.5% levels for the total mass in each cut.

of how efficiently feedback is generating outflows, is roughly an order of magnitude larger during the bursts of star formation from $z = 4 - 2$, expelling a large amount of gas from the disc early on. The resulting suppression of high-redshift star formation is key to obtaining the correct stellar mass relation as the halo grows, is unmistakable in figure 5 and 6. Evidence of these outflows can be seen in the $z = 0$ column density images in figure 2. High-latitude neutral hydrogen from both ejected and infalling material can be seen in the two superbubble cases, but is totally absent otherwise. The smaller amount seen around the high feedback energy case is simply due to this gas being expelled further. The reason superbubbles are so effective at removing mass from the galaxy and thus regulating the stellar mass depends both on the higher outflow rates as well as the lower star formation rates needed to drive these outflows, leading to much larger mass loading factors than the blastwave model can achieve. This is clearly shown in figure 9, as the top panel is essentially the middle panel divided by the bottom panel. The outflow rates driven by superbubbles is at most ~ 2 times greater than the blastwave model, but since this is driven by a comparatively tiny amount of star formation, the massloading, η , is nearly 10 times greater at high redshift. The factor of ~ 2 higher outflow rate is what we would

expect from the roughly ~ 2 larger baryon depletion from the superbubble vs. blastwave cases.

The effectiveness of the superbubble-driven galactic winds can be clearly seen in figure 10, where the net accretion of stars and gas is greatly reduced by the use of superbubble feedback, resulting at $z = 1$ in a net reduction in the total baryonic mass inside $0.5R_{vir}$ of $\sim 14\%$ vs. blastwave feedback, and $\sim 30\%$ vs. no feedback whatsoever (along with the removal of baryons from the disc discussed earlier. As the outflow rate drops towards $z = 0$, much of this ejected material falls back onto the disc, and the outflows transition to a fountain mode, actually increasing the inflow rate seen compared to the blastwave feedback case in figure 11. This increase in the accretion of gas fuels an equivalent increase in star formation, as is seen in figures 7 and 9.

Figure 12 shows that the total accreted gas switches from being dominated by low angular momentum material to being primarily high angular momentum material at $z \approx 2$. Because η is high (~ 10) during this period, low-angular momentum material is preferentially ejected from the galaxy without forming a significant number of stars. These results agree quite well with the results of Muratov et al. (2015), which also found L^* progenitors at $z > 2$ had wind mass loadings $\eta \sim 10$. The preferential ejection of low angular momentum gas is clear in figure 13. The small amount of high angular momentum material accreted before $z = 1$ is ejected at an essentially equal rate with or without superbubble-driven winds, but low angular momentum material is propelled into winds at roughly twice the rate when superbubble feedback is taken into account.

The phase diagram in figure 14 shows that, as expected, the galaxy contains both a hot halo (in which nearly half of the gas mass can be found), and contains no gas in regions of short cooling time. This behavior was shown previously in the isolated galaxy simulations of Keller et al. (2014). The hot halo gas can be divided into three major components. The coolest component is pristine, virial shocked material that has not ever been accreted (never passed within $0.1R_{vir}$ of the halo center). The hottest gas is actually not yet in the corona, but is the interior of young superbubbles still within the galaxy disc. As this material leaves the disc, it cools adiabatically in the lower pressure environment of the halo, as can be seen in from the $\rho^{2/3}$ adiabatic path it takes through the phase diagram. Detailed analysis of this halo gas, especially in comparison to observations like those of Steidel et al. (2010), will be explored in a future study of a larger sample of L^* galaxies.

4 DISCUSSION

Past work, especially the Aquila comparison (Scannapieco et al. 2012), has shown that feedback mechanisms which do not remove a large fraction of baryons from galaxy discs fail to produce realistic spiral galaxies. Galaxies simulated without such feedback show more spheroidal stellar distributions, older stellar populations, and more total stellar mass than is observed in nature. Those cases that do manage to expel enough gas to produce reasonable stellar mass fractions still fail to produce the correct stellar kinematics, failing to produce the small bulges

characteristic of so many spiral galaxies. These models also rely on mechanisms other than stellar feedback (SMBH heating) or on major numerical contrivances (hydrodynamic decoupling, etc.).

Superbubbles offer a way out of this bind. As was shown in (Keller et al. 2014), evaporation in superbubbles naturally mass load winds with temperatures of $\sim 10^7$ K, a process that is set by self-regulating thermal conduction. This means that an optimal amount of material is heated above the virial temperature (1.3×10^6 K for a $8 \times 10^{11} M_\odot$ halo). This feedback-heated and highly buoyant hot gas migrates out of the disc, cooling adiabatically while it rises, as is clearly seen in figure 14. In fact, as figure 6 shows, there may even be room to *reduce* the feedback energy below the fiducial 10^{51} erg/SNe, while still producing reasonable stellar mass fractions. On top of yielding physically-realistic galaxies, superbubble feedback is in fact slightly *less* computationally expensive than blastwave feedback for these simulations, due in part to its elimination of unphysical high density, high temperature gas.

4.1 High-Redshift Outflows Determine Galaxy Properties

A major failure of other feedback models is the production of too many stars, too early. Superbubble feedback prevents this by efficiently removing gas from the star forming disc at high redshifts. The high mass loadings from $z = 2-4$ means more mass is being expelled by significantly fewer stars. Mass loadings much larger than unity have been observed in both Lyman Break Galaxies at high redshift (Pettini et al. 2002) and in local dwarf starbursts (Martin et al. 2002).

Even if a galaxy has the correct stellar mass fraction at $z = 0$, forming too much of your stellar mass at high redshift is problematic for a number of reasons. First, it is known from abundance matching as well as the observations of stellar ages that most stars in L^* galaxies are formed fairly late (e.g. van Dokkum et al. (2013) found $\sim 90\%$ of stars in Milky Way like galaxies formed at $z < 2.5$). Secondly, forming these stars early on means they will be formed primarily in smaller halos that are subsequently accreted, as well as in main halo at small radii (as low angular momentum material is accreted first, as seen in figure 12). This results in a stellar distribution too spheroidal and centrally concentrated, as was seen in many older simulations, and here in the rotation curves in figure 3 for the blastwave and no feedback test cases.

Because superbubbles drive strong outflows at high redshift, the galaxy is able to preferentially remove low angular momentum gas, as indicated by figure 13. This same mechanism was seen in simulations of dwarf galaxies by Brook et al. (2011, 2012). We would suggest that this is a universal requirement for producing galaxies with low central concentrations and small bulges. As Binney et al. (2001) argued, if this gas were to remain within the disc, it would be ultimately form the massive bulge that is seen in our blastwave and no feedback cases, and in numerous other past simulations. If only a third of the baryons removed in the disc of our fiducial case were to instead form bulge stars, it would raise the B/T ratio of the disc to 0.3, making our disc much more bulge dominated than the Milky Way, and putting our results in conflict with Allen et al. (2006). This mech-

anism (strong, high-redshift outflows), and the fact that it produces strong suppression of star formation at high redshift as well as a small stellar bulge, agrees well with the results of Sales et al. (2012). That study of ~ 100 GIMIC (Crain et al. 2009) galaxies found that those with the smallest B/T ratio also had the largest fraction of stars formed late in the galaxy’s history. Strong outflows acting to regulate high redshift star-formation while preserving fuel for late star formation naturally leads to this situation.

The effectiveness of superbubble feedback may help to prevent the growth of a massive stellar bulge via a second mechanism as well. Fall & Efstathiou (1980) showed that the dissipational collapse of hot gas within an extended dark halo can produce galaxies with thin discs. However, Cole et al. (2000) showed that the collisionless processes involved in galaxy mergers can cancel out the net rotation of a galaxy disc and lead to a spheroidal stellar distribution. With superbubble feedback, small dwarves convert very little of their baryonic mass into stars, allowing them to contribute their gas to the primary halo, which then collapses dissipationally.

The heavily mass loaded winds driven by superbubble feedback are not only key to suppressing high- z star formation, but also to providing enough gas at low redshift to continue star formation. The outflows produced by superbubble feedback can easily escape from the lower-mass progenitors of L^* galaxies. Thus it is able to naturally transition from the violent, wind-driving high redshift mode to a more quiescent phase as the galactic gravitational potential and gas surface densities in the disc increase (see the increase in inflow in figure 11. These factors suppress outflows, and allow star formation to increase slowly towards $z = 0$.

As the disc is assembled, the disc surface density above the superbubble increases. Thus the hot gas must push past more material and will also entrain more material along with it as shown by the clumps seen in figure 2). This slows the outflows compared to those seen at high redshift and moving the galaxy towards a fountain mode. The gas is kicked to relatively low altitudes and then rains back down onto the galactic disc. This effect is probably sensitive to resolution. Our small-scale experiments show that venting of superbubbles is enhanced by a more porous ISM (see Keller et al. 2014 and also Nath & Shchekinov 2013). Poor resolution suppresses this porosity and increases numerical dissipation. Thus better resolution might reduce the puffy appearance in the HI column density and allow strong galactic outflows towards $z = 0$.

4.2 Additional Feedback Mechanisms

We have shown that, even at moderate resolution, thermal supernova feedback is sufficient to build a realistic L^* galaxy, provided a complete physical feedback model like that of Keller et al. (2014) is used. Thus this work firmly establishes what supernovae and superbubbles can do.

It is still likely that for higher-mass halos ($> 10^{12} M_\odot$), supernovae alone will not be sufficient to regulate star formation and produce the drop in star formation efficiency seen in Moster et al. (2013); Behroozi et al. (2013). We do not include feedback from SMBH, which is likely to be important for higher-mass galaxies.

Our resolution limits the formation of dense structures

in the ISM. The lack of resolved dense gas means that feedback processes involved in disrupting molecular clouds (UV photodissociation, radiation pressure, etc.) is largely irrelevant for these simulations. In fact, since much of the energy from early stellar feedback is consumed in the disruption of the densest clouds in simulations such as this, the addition of this energy may be unrealistic, effectively double counting energy that would have been used to disrupt clouds. Furthermore, high-resolution studies of individual molecular clouds have found that ionizing radiation, despite disrupting these clouds, ultimately only imparts $\lesssim 0.1\%$ of the total radiative luminosity to the gas in the cloud and the surrounding medium in the form of additional thermal and kinetic energy (Dale et al. 2005; Gendele & Krumholz 2012; Walch et al. 2012)). Thus, applying even as little as 1% of the radiative luminosity as a source of feedback in a simulation that does not resolve structure within molecular clouds is likely massively overestimating the impact on disc scales.

In sufficiently high-resolution simulations it may be necessary to include small scale feedback mechanisms in order to disrupt clouds before the first SN, allowing the to explode in a lower density environment since, as Mac Low & McCray (1988) showed, the cooling time for superbubbles scales sub-linearly with the inverse density, $t_R \propto n_0^{-8/11}$. Rogers & Pittard (2013) showed that the disruption of high-density clouds by stellar winds prior to the first supernovae can allow as much as 99% of the hot SN ejecta to escape into the surrounding warm ISM, helping to promote the growth of superbubbles that then vent from the galactic disc. In the current work, the densities near the superbubbles are modest and this preprocessing is not required.

5 CONCLUSION

We have shown that supernova feedback alone, with a complete physical superbubble model, is capable of producing an L^* galaxy that falls within observational constraints. Superbubbles are a physical mechanism for producing ab initio galactic winds, that ultimately allow for the formation of a galaxy with a realistic star formation history and a negligible stellar bulge.

The key results with respect to galaxy formation are as follows:

- Strong outflows at high redshift are essential to regulating star formation over the total halo history. The vast majority of stars in L^* galaxies form after $z \sim 2$. Unless gas is removed from galaxies at high redshift by feedback processes, it will rapidly form stars, yielding discs that are too massive and red at $z = 0$.
- Outflows are important for producing the correct disc kinematics and preventing the formation of excessive bulges. Low angular momentum gas is accreted first as galaxies form, and the pooling of this gas at the center of galaxies can lead to galaxies with sharply peaked rotation curves and unrealistically large bulges, often containing the majority of stars within the galaxy.
- Galaxies simulated without feedback, or with disabled cooling feedback models fail to expel enough of this gas early on, and result in bulge-dominated galaxies with unrealistic stellar mass fractions. The superbubble model, on the other

hand, produces strong outflows that ultimately yield realistic galaxies.

- Superbubble feedback naturally yields the sort of outflows that are required for L^* galaxies. The mass-loading & velocity of the winds are set by the hydrodynamics and evaporative mixing, unlike other methods where these values are free parameters.
- Superbubble feedback produces high-redshift outflows that preferentially remove low angular momentum gas, and in so doing, prevents the formation of massive bulges and the associated strongly peaked rotation curves. It does this without also expelling additional high-angular momentum gas, allowing the stellar disc to form while arresting the formation of a bulge.
- These advantages come without any significant additional computational expense, and may in fact be less costly than alternative feedback models.

Superbubbles are effective up to at least L^* . Beyond L^* , we anticipate important roles for SMBH feedback or potentially radiation pressure (see e.g. Hopkins 2013). In the subsequent MUGS2 series of papers, we will show how these effects extend to larger and smaller halos forming in a range of environments.

ACKNOWLEDGEMENTS

The analysis was performed using the pynbody package (<http://pynbody.github.io/>, (Pontzen et al. 2013)), which was written by Andrew Pontzen in addition to the authors. We thank Fabio Governato, Tom Quinn, Sijing Shen, Greg Stinson, & Rob Thacker for useful conversations regarding this paper. The simulations were performed on the clusters hosted on SCINET, part of ComputeCanada. We greatly appreciate the contributions of these computing allocations. We also thank NSERC for funding supporting this research.

REFERENCES

- Abadi M. G., Navarro J. F., Steinmetz M., Eke V. R., 2003, *ApJ*, **591**, 499
- Agertz O., Kravtsov A. V., 2014, preprint, ([arXiv:1404.2613](https://arxiv.org/abs/1404.2613))
- Agertz O., et al., 2007, *MNRAS*, **380**, 963
- Agertz O., Kravtsov A. V., Leitner S. N., Gnedin N. Y., 2013, *ApJ*, **770**, 25
- Allen P. D., Driver S. P., Graham A. W., Cameron E., Liske J., de Propriis R., 2006, *MNRAS*, **371**, 2
- Anglés-Alcázar D., Davé R., Özel F., Oppenheimer B. D., 2014, *ApJ*, **782**, 84
- Aumer M., White S. D. M., Naab T., Scannapieco C., 2013, *MNRAS*, **434**, 3142
- Behroozi P. S., Wechsler R. H., Conroy C., 2013, *ApJ*, **770**, 57
- Binney J., Gerhard O., Silk J., 2001, *MNRAS*, **321**, 471
- Bower R. G., Benson A. J., Malbon R., Helly J. C., Frenk C. S., Baugh C. M., Cole S., Lacey C. G., 2006, *MNRAS*, **370**, 645
- Breitschwerdt D., McKenzie J. F., Voelk H. J., 1991, *A&A*, **245**, 79
- Brook C. B., et al., 2011, *MNRAS*, **415**, 1051
- Brook C. B., Stinson G., Gibson B. K., Roškar R., Wadsley J., Quinn T., 2012, *MNRAS*, **419**, 771
- Brooks A. M., et al., 2011, *ApJ*, **728**, 51
- Chabrier G., 2003, *PASP*, **115**, 763

- Christensen C. R., Brooks A. M., Fisher D. B., Governato F., McCleary J., Quinn T. R., Shen S., Wadsley J., 2014, *MNRAS*, **440**, L51
- Cole S., Lacey C. G., Baugh C. M., Frenk C. S., 2000, *MNRAS*, **319**, 168
- Crain R. A., et al., 2009, *MNRAS*, **399**, 1773
- Creasey P., Theuns T., Bower R. G., Lacey C. G., 2011, *MNRAS*, **415**, 3706
- Dale J. E., Bonnell I. A., Clarke C. J., Bate M. R., 2005, *MNRAS*, **358**, 291
- Dalla Vecchia C., Schaye J., 2012, *MNRAS*, **426**, 140
- Dekel A., Birnboim Y., 2006, *MNRAS*, **368**, 2
- Durier F., Dalla Vecchia C., 2012, *MNRAS*, **419**, 465
- Fall S. M., Efstathiou G., 1980, *MNRAS*, **193**, 189
- Ferland G. J., et al., 2013, *RMxAA*, **49**, 137
- Gendele L., Krumholz M. R., 2012, *ApJ*, **745**, 158
- Genzel R., et al., 2011, *ApJ*, **733**, 101
- Governato F., et al., 2004, *ApJ*, **607**, 688
- Governato F., et al., 2009, *MNRAS*, **398**, 312
- Guedes J., Callegari S., Madau P., Mayer L., 2011, *ApJ*, **742**, 76
- Heckman T. M., Armus L., Miley G. K., 1987, *AJ*, **93**, 276
- Hopkins P. F., 2013, *MNRAS*, **428**, 2840
- Ipavich F. M., 1975, *ApJ*, **196**, 107
- Katz N., White S. D. M., 1993, *ApJ*, **412**, 455
- Kauffmann G., Colberg J. M., Diaferio A., White S. D. M., 1999, *MNRAS*, **303**, 188
- Keller B. W., Wadsley J., Benincasa S. M., Couchman H. M. P., 2014, *MNRAS*, **442**, 3013
- Knollmann S. R., Knebe A., 2009, *ApJS*, **182**, 608
- Krumholz M. R., Thompson T. A., 2013, *MNRAS*, **434**, 2329
- Larson R. B., 1974, *MNRAS*, **169**, 229
- Leitherer C., et al., 1999, *ApJS*, **123**, 3
- Mac Low M.-M., McCray R., 1988, *ApJ*, **324**, 776
- Marasco A., Fraternali F., Binney J. J., 2012, *MNRAS*, **419**, 1107
- Martin C. L., Kobulnicky H. A., Heckman T. M., 2002, *ApJ*, **574**, 663
- Martin C. L., Shapley A. E., Coil A. L., Kornei K. A., Bundy K., Weiner B. J., Noeske K. G., Schiminovich D., 2012, *ApJ*, **760**, 127
- Mathews W. G., Baker J. C., 1971, *ApJ*, **170**, 241
- Moster B. P., Naab T., White S. D. M., 2013, *MNRAS*, **428**, 3121
- Munshi F., et al., 2013, *ApJ*, **766**, 56
- Muratov A. L., Keres D., Faucher-Giguere C.-A., Hopkins P. F., Quataert E., Murray N., 2015, preprint, ([arXiv:1501.03155](https://arxiv.org/abs/1501.03155))
- Murray N., Quataert E., Thompson T. A., 2005, *ApJ*, **618**, 569
- Nath B. B., Shchekinov Y., 2013, *ApJ*, **777**, L12
- Newman S. F., et al., 2012, *ApJ*, **761**, 43
- Pettini M., Rix S. A., Steidel C. C., Adelberger K. L., Hunt M. P., Shapley A. E., 2002, *ApJ*, **569**, 742
- Pontzen A., Roškar R., Stinson G. S., Woods R., Reed D. M., Coles J., Quinn T. R., 2013, pynbody: Astrophysics Simulation Analysis for Python
- Rees M. J., Ostriker J. P., 1977, *MNRAS*, **179**, 541
- Ritchie B. W., Thomas P. A., 2001, *MNRAS*, **323**, 743
- Robertson B. E., Kravtsov A. V., 2008, *ApJ*, **680**, 1083
- Rogers H., Pittard J. M., 2013, *MNRAS*, **431**, 1337
- Sales L. V., Navarro J. F., Theuns T., Schaye J., White S. D. M., Frenk C. S., Crain R. A., Dalla Vecchia C., 2012, *MNRAS*, **423**, 1544
- Scannapieco C., et al., 2012, *MNRAS*, **423**, 1726
- Schaye J., et al., 2015, *MNRAS*, **446**, 521
- Shen S., Wadsley J., Stinson G., 2010, *MNRAS*, **407**, 1581
- Socrates A., Davis S. W., Ramirez-Ruiz E., 2008, *ApJ*, **687**, 202
- Springel V., Hernquist L., 2003, *MNRAS*, **339**, 289
- Steidel C. C., Erb D. K., Shapley A. E., Pettini M., Reddy N., Bogosavljević M., Rudie G. C., Rakic O., 2010, *ApJ*, **717**, 289
- Stinson G., Seth A., Katz N., Wadsley J., Governato F., Quinn T., 2006, *MNRAS*, **373**, 1074
- Stinson G. S., Bailin J., Couchman H., Wadsley J., Shen S., Nickerson S., Brook C., Quinn T., 2010, *MNRAS*, **408**, 812
- Stinson G. S., Brook C., Macciò A. V., Wadsley J., Quinn T. R., Couchman H. M. P., 2013, *MNRAS*, **428**, 129
- Thacker R. J., Couchman H. M. P., 2000, *ApJ*, **545**, 728
- Veilleux S., Cecil G., Bland-Hawthorn J., 2005, *ARAA*, **43**, 769
- Vogelsberger M., Genel S., Sijacki D., Torrey P., Springel V., Hernquist L., 2013, *MNRAS*, **436**, 3031
- Wadsley J. W., Stadel J., Quinn T., 2004, *New Astronomy*, **9**, 137
- Walch S. K., Whitworth A. P., Bisbas T., Wünsch R., Hubber D., 2012, *MNRAS*, **427**, 625
- Weiner B. J., et al., 2009, *ApJ*, **692**, 187
- White S. D. M., Rees M. J., 1978, *MNRAS*, **183**, 341
- Woods R. M., Wadsley J., Couchman H. M. P., Stinson G., Shen S., 2014, *MNRAS*, **442**, 732
- van Dokkum P. G., et al., 2013, *ApJ*, **771**, L35